Hydrodynamic simulation of frontal plane deck motion during a mechanical shock on a lifeboat

Jens Thiele, Ya Huang*, Jason Knight
School of Mechanical & Design Engineering
University of Portsmouth
Portsmouth, UK

***Abstract*—Multi-axial repeated mechanical shocks presented in the frontal plane of any planing crafts during sea transits impose an increased risk to injury for occupants. However, understanding of the abrupt motion in this plane is seldom documented in adequate detail. With the help of computational fluidic dynamics (CFD) software, the study simulates the boat motion during different water entry conditions. An Atlantic 21 lifeboat is dropped into water with different drop heights and entry roll angles in simulation. The vertical, lateral and angular roll acceleration of the lifeboat are derived from the CFD simulations. The vertical acceleration calculated at a crew seat is considerably higher than that at the boat centre of mass (CoM) in the frontal plane. The percentage increase from the offset position relative to the CoM is primarily governed by the entry roll angle with little influence from the drop height. The lateral acceleration is less critical when assessing mechanical shocks in the frontal plane, as it is largely cancelled by the lateral component due to the offset and the roll angular acceleration.**

Keywords—mechanical shock, high-speed marine crafts, drop tests, hydrodynamic simulation

I. Introduction

In heavy seas, 'wave slams' induce high-acceleration events exposing occupants to mechanical shocks and whole-body vibration of extreme magnitudes. The repeated impulsive load is a constant health threat to the human musculoskeletal system with both acute and chronic impact on the operators of high speed marine crafts across the entire maritime workforce, from offshore windfarms, search and rescue, to military operations.

The response of the boat during an asymmetric drop under a certain impact angle in the frontal plane around the longitudinal axis of the craft (x) is particularly dangerous to human occupants. The human spine is primarily evolved to extend and flex in the mid-sagittal plane but with limited rotational freedom in the frontal plane [1]. The dominant human response to shock and vibration research has been limited to translational vertical and horizontal motion, partly due to the physical constraints of existing equipment and environment to reproduce the abrupt shock motion at sea with the correct magnitude and frequency contents. Sea trials and boat drop tests carries a large time and cost penalty with a possibility to induce hazardous motion to the crew [2]. A more controllable and economical approach to generate realistic deck response motion during a shock at sea would be to simulate the fluid-structure interaction using a known hull form with a computational fluidic dynamics (CFD) package. The drop height, entry angle, and flow speed can be combined to control the deck motion (Fig 1). This serves as the excitation to drive human biomechanical models to evaluate any loading on the musculoskeletal system.

* Correspondence author: Ya Huang (ya.huang@poet.ac.uk)

For the fluid-hull interaction, the braking force at the free water surface entry depends on a number of factors. An analytical prediction of the vertical hull entry for a complex three-dimensional hull design is not possible. This study will focus on a numerical approach using different impact velocity and the entry angle in the frontal plane. The general approach has been to solve the flow around a two-dimensional wedge entering the water surface with a constant velocity iteratively to solve the equations for the pressure distribution on the wedge [3]. It is based on a nonlinear boundary element method (BEM) with a jet flow approximation for symmetrical impact in the frontal plane. Asymmetric impacts of a three-dimensional wedge entering the water surface with different initial roll angles can be solved using a combination of experimental approach such as the particle image velocimetry (PIV) and an iterative solution [4]. But full analytical solution is usually not achievable when the flow begins to separate from the wedge for impact angels larger than 30°. There has been a strong correlation between the hydrodynamic load and the entry angle.

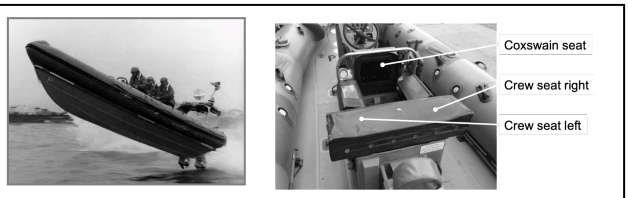

Fig 1 A freefall and wave slam of a RIB transit, Clacton, RNLI (left), and the seating arrange for an Atlantic 21 (right).

The vertical hull entry can usually be characterized by an acceleration profile at the centre of mass (Fig 2). Phase A features a freefall and a constant negative acceleration of 1 g. Phase B depicts the primary impact usually last for 50 to 75 ms [5]. This is usually a highly non-linear phases with

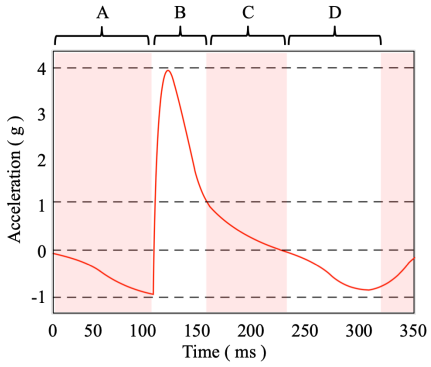

Fig 2 Schematic example vertical acceleration history measured at the mass centre showing different phases during a hull-fluid mechanical shock: A) primary drop – freefall; B) impact; C) inertial effect; D) secondary drop.

complicated local propagation of structural borne mechanical waves. In phase C, the boat hull is still partly supported by water, displaying a positive acceleration less than 1 g, until it heaves out after this stage. Peak upward velocity could emerge at the end of C. The hull starts the secondary fall from phase D where the maximum downward displacement would occur. So far, the drop tests and simulations have been focused on the dominant vertical acceleration and force generated by the impact [2, 5]. To the author's knowledge, no work has been reported in the ensuing lateral and roll axes on the deck level.

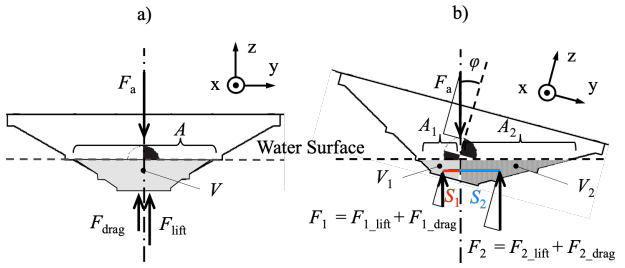

Fig 3 Free body diagrams of the rigid hull (A21) in the frontal view with initially zero (a) and tilted roll angle φ about the x-axis (b) – notice the orthogonal components of F_a, F_1 and F_2 in the tilted coordinate system, i.e. the body frame attached to the hull.

Simulating the three-dimensional fluid-hull interaction is complex with cumbersome computational and time costs, which increase with any new hull form and hull size developed [6]. One way to reduce these costs is to focus on the motion and force in the frontal plane where the human occupant is the most vulnerable. The behaviours of rough waves in combination with boat heading, speed and hydrodynamic properties are challenging and measurements do not often give reproducible results for further investigations. The present study therefore analyses a series of specifically defined drops from a range of heights under different impact angles defined in the frontal plane of the boat. They are based on the hydrodynamic hull form and behaviour of a rigid inflatable boat (RIB) Atlantic 21 (A21) lifeboat developed by the Atlantic College (Wales) and used by the Royal National Lifeboat Institution (RNLI, UK). A crew is usually formed of three people, while one of them controls the boat at the front while the other two sit behind. The A21 series served the RNLI until 2008 and has been replaced by the newer Atlantic 75, which has comparable specifications in terms of shape and performance. The study considers the hull form of the A21 (length: 7.38 m; beam 2.65m; draught: 0.41 m; deadrise angle in the frontal plane: approximately 20 deg; mass: 1600 kg).

The aim is to provide a simple process using off-the-shelf software packages such as STAR-CCM® [7] to obtain three-dimensional hydrodynamic characteristics during typical wave slam impacts based on an A21 lifeboat or any given hull form. In the frontal plane, the roll angular acceleration, lateral and vertical accelerations will be analysed for different drop heights and initial entry roll angles to the free water surface. The CFD simulation results can be used for computer aided engineering to develop new shock suspension seats and shock mitigation solutions for both motion sensitive equipment, structure and human occupants.

II. Methodology

To determine the rigid body motion of a boat at the deck level during an impact with water in the frontal plane, one requires three equations of motions and a free body diagram (FBD) to illustrate all forces and moments (Fig 3). Some of the forces have to be derived from the fluid-hull interaction problem numerically. The chosen parameters for the CFD simulation and solution need to be defined and explained using the STAR-CCM® software. This section will summarize these aspects of the simulation work. The Newtonian (dot) style of time differentiation is adopted.

A. Hull equations of motion at water entry

The resultant motion need to be analytically derived from all forces and their ensuing moments acting on the boat hull during the impact in the frontal plane. Hydrodynamic lift due to buoyancy and hydrodynamic drag, both acting in the vertical axis of the earth inertial frame, are the two primary fluidic forces to be extracted from the pressure acting on the hull surface [8]. It is this pressure time history distributed on the hull surface that will be resolved from the CFD simulation. Opposing these fluidic forces is the inertia force due to the mass of the boat also acting in the vertical axis (Fig 3).

With zero roll angle during the impact, albeit how unlikely this could be the case, the three equations of motion in the frontal plane can be reduced to just one for the total resultant force in the vertical z-axis ($\sum F_z$). This is because all forces in the lateral y-axis does not exist, neither does any moment about the x-axis as all forces, be it the inertial force, hydrodynamic drag or lift, pass through the mass centre where the moment is taken (Fig 3a). The equation of motion at every incremental time of equilibrium for this condition becomes (with reference to Table I):

$$\sum F_z = F_a + F_{lift} + F_{drag} = 0 \quad (1)$$

where

$$F_a = m \cdot \ddot{z}(t) \quad (2)$$

$$F_{lift} = \rho_w \cdot g \cdot V(z,t) \quad (3)$$

$$F_{drag} = \tfrac{1}{2} \cdot \rho_w \cdot A(z,t) \cdot \dot{z}(t)^2 \quad (4)$$

With an initially tilted roll angle at the impact, the three equations of motion in the frontal plane are required at every incremental time to establish the equilibrium for vertical resultant force in the z-axis ($\sum F_z$), lateral resultant force in the y-axis ($\sum F_y$), and roll moment about the x-axis ($\sum M_x$) respectively with reference to Fig 3b:

$$\sum F_z = F_a \cdot \cos\varphi + F_1 \cdot \cos\varphi + F_2 \cdot \cos\varphi = 0 \quad (5)$$

$$\sum F_y = F_a \cdot \sin\varphi + F_1 \cdot \sin\varphi + F_2 \cdot \sin\varphi = 0 \quad (6)$$

$$\sum M_x = M_a + F_1 \cdot S_1 + F_2 \cdot S_2 = 0 \quad (7)$$

where

$$M_a = I_{xx} \cdot \ddot{\varphi}(t) \quad (8)$$

$$F_1 = F_{1\_lift} + F_{1\_drag} \quad (9)$$

$$F_2 = F_{2\_lift} + F_{2\_drag} \quad (10)$$

$$F_{1\_lift} = \rho_w \cdot g \cdot V_1 \quad (11)$$

$$F_{2\_lift} = \rho_w \cdot g \cdot V_2 \quad (12)$$

$$F_{1\_drag} = \tfrac{1}{2} \cdot \rho_w \cdot A_1 \cdot \dot{z}(t)^2 \quad (13)$$

$$F_{2\_drag} = \tfrac{1}{2} \cdot \rho_w \cdot A_2 \cdot \dot{z}(t)^2 \quad (14)$$

Due to the roll angular acceleration about the x-axis on the rigid body hull, any location of interest in the frontal plane away from the mass centre will experience different translational tangential accelerations in the vertical z- and lateral y-axis. It is therefore necessary to define the distances between the location of interest and the orthogonal axis passing the mass centre – both highlighted in Fig 4.

TABLE I. NOTATIONS FOR EQUATIONS OF MOTION

$\ddot{z}(t), \dot{z}(t), z(t)$ $\ddot{y}(t), \dot{y}(t), y(t)$ $\ddot{x}(t), \dot{x}(t), x(t)$	Vertical translational (z) acceleration, velocity, position, and similarly for lateral translational (y) and longitudinal translational (x) (Fig 3, 4)
$\ddot{\varphi}(t), \dot{\varphi}(t), \varphi(t)$	Roll angular acceleration, velocity, displacement about the longitudinal x-axis (Fig 3, 4)
t	Time scale (Fig 3, 4)
$V(z,t)$	Total submerged volume of the hull as a function of longitudinal position z and time t (Fig 3a)
V_1, V_2	Left and right submerged volume of the hull respectively (Fig 3b)
$A(z,t)$	Total cross sectional area of the hull in the x-y plane at the water level as a function of longitudinal position z and time t (Fig 3a)
A_1, A_2	Left and right cross sectional area of the hull in the x-y plane at the water level respectively (Fig 3b)
F_a	Inertial force due to boat mass and translational acceleration $\ddot{z}(t)$ (Fig 3)
M_a	Inertial moment due to boat mass moment of inertia about the x-axis and angular acceleration $\ddot{\varphi}(t)$
F_1, F_2	Left and right hydrodynamic forces due to lift (F_{1_lift}, F_{2_lift}) and drag (F_{1_drag}, F_{2_drag}) respectively in Fig 3b
F_{lift}	Hydrodynamic lift (buoyancy) from fluid-hull interaction
F_{drag}	Hydrodynamic drag from fluid-hull interaction
S_1	Left lever arm of F_1 about the mass centre (Fig 3b)
S_2	Right lever arm of F_2 about the mass centre (Fig 3b)
d_y	y component of the distance to the z-axis (Fig 4a)
d_z	z component of the distance to the y-axis (Fig 4b)
g	Gravitational acceleration
ρ_w	Density of water
m	Mass of the boat
I_{xx}	Mass moment of inertia of the boat about the x-axis

The resultant translational acceleration of the lateral locations of interest in the vertical z-axis of the boat becomes (Fig 4a):

$$\ddot{z}_i(t) = \ddot{\varphi}(t) \cdot d_y + \ddot{z}(t) \qquad (15)$$

The resultant translational acceleration of the vertical locations of interest in the lateral y-axis is (Fig 4b):

$$\ddot{y}_i(t) = \ddot{\varphi}(t) \cdot d_z + \ddot{y}(t) \qquad (16)$$

The distance d_y is measured between the lateral location of interest in the lateral y-axis and the perpendicular z-axis passing the boat mass centre (Fig 4a). Physically this represents the lateral distance of the mass centre of a crew to the z-axis, usually in the range [-5, 5] m in the y-axis. The distance d_z is measured between the vertical location of interest in the vertical z-axis and the perpendicular y-axis passing the boat mass centre (Fig 4b). It represents the vertical distance of the mass centre of a crew to the y-axis, usually governed by the crew's sitting height in the range [0.5, 1] m in the z-axis.

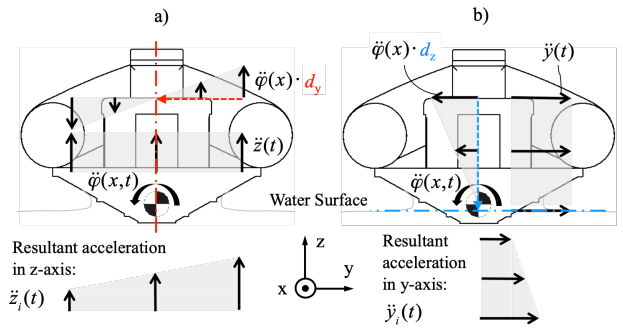

Fig 4 Frontal plane rigid body kinematics (A21) for a) vertical z-axis resultant motion derived from roll (φ about x) angular acceleration, y component of the distance to the z-axis (d_y) and vertical (z) acceleration, and b) lateral y-axis resultant motion derived from roll (φ about x) angular acceleration, z component of the distance to the y-axis (d_z) and lateral (y) acceleration.

By treating the boat as a rigid body in the frontal plane, the angular motion of the boat can be derived directly from the pressure distribution and resulting moments acting upon the hull; the translational motion at different locations of interest on the boat can then be calculated by adding the tangential components at that location due to rotation using Eq (15) and (16) to the translational motion at the boat mass centre.

The paper derives all equations from the boat centre of mass (CoM), but the boat local coordinate system for the CFD results was based on x = 0.5 m, y = 0 m and z = 1 m respectively to the CoM.

B. CFD simulation setup

The CFD simulation computes the pressure, force and moment acting on the full hull so as to derive motion on the boat using the analytical solution above. A general guidance on the procedure for a CFD work flow can be found at Appendix A for the reader's convenience. The setup of the present simulation will primarily follow an example using the STAR-CCM® and its dynamic fluid body interaction (DFBI) to create a 6DoF rigid boat model [7].

The simulation starts by importing the 3D CAD model automatically prepared using self-intersecting and fully solved faces. The boundary conditions for the boat drop require an inlet, outlet and wall interface. The mesh is generated to approximate the entire domain by a simple element shape grid. The physics model of the fluid-structure interaction is then configured. The solver needs to be set to reflect whether the flow is dynamic or steady state. Before running the simulation, "monitors" and "scenes" can be set up to visualise the solution.

1) Boat CAD model and import

The boat hull is generated using Autodesk Inventor® based on a RNLI A21 technical drawing. To design a complex boat hull, it is necessary to produce several section planes along the length of the hull (Fig 5a). It is possible to modify the hull design to tune the drag and impact characteristics.

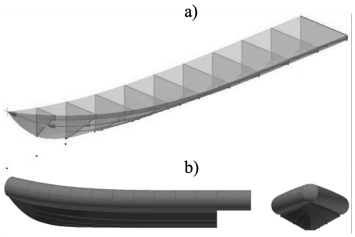

Fig 5 Section plane of an A21 hull (a); 3D model (b)

After generating the hull, the tube is expanded from a circle sketch along the longitudinal direction of the deck edge. Modelling the tube is necessary, as the draught for high drops can be larger than the hull height. In reality the tube is made up of elastic materials. However, the tube pressure was found to have insignificant influence on the dynamic motion of the rigid hull. Therefore, the tube is simplified to be rigid and is rigidly attached to the hull [6].

2) Physics

The simulation of a boat drop in the air and impact with the free water surface requires a multiphase fluid, i.e. air and water, and a motion environment. The air and water are treated as Eulerian phases with constant density. The solver is configured to be implicit unsteady as the system does not reach equilibrium (Table II).

TABLE II. PHYSICS SETTINGS

Solver	Segregated
Time	Implicit Unsteady
Material	Eulerian Multiphase
Multiphase Model	Volume of Fluid (VOF)
Viscous Regime	Turbulent
Reynolds-Averaged Turbulence	κ-ε-Turbulence Two-Layer
Optional Models	Gravity VOF Waves

Solver

The hydrodynamic equations can either be solved by iteration via steady states or by time-stepping as an unsteady solution. As the results from the lifeboat drop simulation were expected to vary over time, the unsteady solver was selected. For a faster computational time, the implicit method was used which employed the segregated model. By defining the stream function Φ(x, y, z, t) as a volume flux in 3D space and as a function (f) of time, one can update the solution with every time-step by considering its partial derivative:

$$\frac{\partial \Phi}{\partial t} = f\big(t, \Phi(x, y, z, t)\big) \tag{17}$$

and evaluate at the next time step by integration:

$$\Phi^{n+1} = \Phi^{n} + \int_{t}^{t+\Delta t} f\big(t, \Phi(x, y, z, t)\big)dt \tag{18}$$

Solving the integral approximated using the value of the integrand at the final time gives the final expression for a fully implicit solution.

$$\Phi^{n+1} = \Phi^{n} f(t + \Delta t, \Phi^{n+1})\Delta t \tag{19}$$

The above cannot be solved analytically as Φ^{n+1} appears on both sides of the equation. Meanwhile the solution of the implicit unsteady solver requires the segregated solver to deal with one equation for the velocity and another for the pressure separately. The segregated flow method solves two additional equations for pressure and velocity according to the Semi-Implicit Method for Pressure Linked Equations (SIMPLE) algorithm commonly used for numerical procedure to solve the Navier-Stokes equations by guessing in an iterative manner.

Material

Describing a free water surface requires the definition of two different fluids with different phase conditions – water for the heavy liquid and air as the light gas fluid. These can be applied using the Eulerian multiphase model in the material section of the software. Both water and air can be treated with constant density and incompressible. Air is regarded incompressible due to the low impact speeds.

The standard technique for physical modelling of a free surface in the boundaries of two phases is the volume of fluid method (VOF). It employs a scalar function to describe the volume fraction of both fluids [10]:

$$\frac{\partial C_m}{\partial t} + u \cdot \nabla C_m = 0 \tag{20}$$

where C_m is the volume fraction of the fluid with a value of "1" when the cell is filled entirely with the heavy fluid water and "0" for the light fluid air; u is flow velocity; ∇ is divergence. For cells at the interface between the two fluids, C_m is between 0 and 1 approximating the state with the Piecewise Linear Interface Construction (PLIC). A more refined mesh in this interface region would increase the fidelity but at a computational cost.

Viscosity regime

During the impact the flow is turbulent in both air and water with a Reynolds Number (Re) from about 7.77×10^6 to 17.4×10^6 (much larger than 2900) based on the beam or width of the boat at 2.49 m, and the entry velocities from about 3 to 7 m/s depending on the various drop heights. These values are greater than the critical Re of a cylinder at 0.35x $\times 10^6$ for turbulent flow. The standard κ-ε-turbulence model is applied to represent the mean flow characteristics of the turbulence during impact. It couples the turbulent kinetic energy κ with the rate of dissipation of the turbulent kinetic energy ε. The transportation equation for κ is:

$$\frac{d\kappa}{dt} = \nabla\left(\frac{v_t}{\sigma_\kappa}\nabla\kappa\right) + \mathrm{p} - \varepsilon \tag{21}$$

and for ε is:

$$\frac{d\varepsilon}{dt} = \nabla\left(\frac{v_t}{\sigma_\varepsilon}\nabla_\varepsilon\right) + C_{\varepsilon_1}\frac{p_\varepsilon}{\kappa} - C_{\varepsilon_2}\frac{\varepsilon^2}{\kappa} \tag{22}$$

Using the κ-ε-turbulence model requires an additional function to solve the results in the sub-layer wall region given by the additional terms with the "Two-Layer All Wall Treatment". By applying the two-layer approach, the dissipation rate and the turbulent viscosity can be specified as functions of the wall distance [11].

Optional models

Optional settings are still required for the present problem: an applied gravity force and a VOF-Waves model. As the dominant driving force of the drop simulation, gravity was defined as a vector of 9.81 m/s^2 in the negative z-axis of the inertial frame.

The waves are defined as "Flat-Waves" resembling a calm water surface with minimal influence from wind and current. Such simplification is based on the boat heave approximated by different drop heights. By applying VOF waves it was possible to set the field functions in STAR-CCM® to associate velocity, pressure and volume fraction during the simulation with the VOF model. The field functions were set in the inlet and outlet boundary conditions. All pressure-related parameters were set in the "Hydrostatic Pressure of Flat Wave" section, while the velocity parameters were in the "Velocity of Flat Wave" section. The volume fraction was divided into a heavy (water) and a light (air) fluid. It is essential that the reference density for the fluids is equal to the initial values [11].

3) Boundaries

Any CFD simulation needs to define the boundary conditions for all external faces of the domain. The inlet and outlet are shown in Fig 6b, whereas all other external surfaces are set as symmetry planes. In addition, the boat itself is treated as a non-slip wall within the water-air fluid domains (Fig 6b). The missing front face in Fig 6b is not shown for better visualisation.

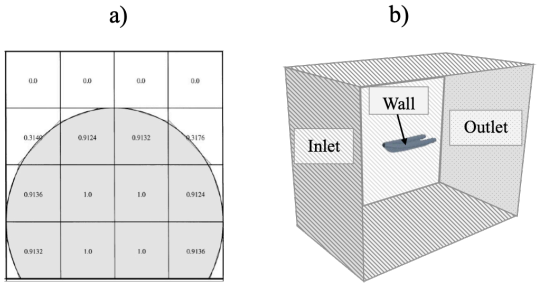

Fig 6 Schematic of the C_m values for VOF method [10] (a); boundaries of the two-phase fluid (b).

4) Dynamic Fluid Body Interaction (DFBI)

In STAR-CCM® the DFBI model describes the 6-degrees-of-freedom (6DoF) rigid body boat motion during the fluid-structure impact, including translations in x-, y- and z-axis, and rotations about each of x-, y- and z-axis. The 6DoF makes the simulation more realistic, but also more computationally expensive. The current study focuses on motions in the frontal plane, so translations in the vertical z-axis and lateral y-axis, and roll about x-axis were enabled in the model. The DFBI solver requires the inertial properties of the boat, i.e. its mass, mass moments of inertia for each enabled rotational axis, and cross products of inertia.

5) Mesh

The three-dimensional problem requires a volume mesh for the entire fluid domain with a surface mesh around the boat which is a non-slip wall boundary. The trimmed cell mesher is used to generate the volume mesh by cutting a hexahedral mesh with the geometry surface. The base mesh is defined by one-metre cubes spread within the entire background domain. Around the boat and the water surface the mesh is refined volumetrically using the custom volumetric control. Five prism layers on the boat are used to refine the mesh around the wall boundary accurately. The arrangement of the refinement blocks can be seen in Fig 7a [11].

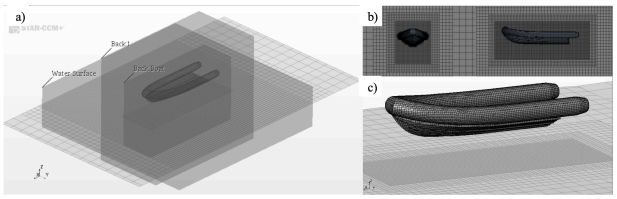

Fig 7 Mesh refinement volumes (a); mesh of water around the boat wall (b); mesh on the boat and water surface (c).

To determine the mesh size and refinement parameters, the space discretisation was evaluated by changing the mesh size and recording the peak acceleration in the simulation iteratively. Firstly, only the base size was varied whilst using the same time step size of 0.01 s. Trials presented in Fig 8a showed that the peak acceleration converged to around 3.3g – as a result of a 1-metre free fall height. The base size of 2 metres resulted in over 1.2 million of cells at a substantial computational cost. To avoid this, the base size was fixed at 4.5 metres, while the refinement parameter around the boat was allowed to reduce until the peak acceleration reaches 3.3g. This procedure generated the final mesh of approximately 440 thousand cells. The wall region was represented by five prism layers with a total thickness of 2% of the base size. These trials were performed with a time step of 0.01s. The effect of time step on the solution and computation time is described in the next sub-section.

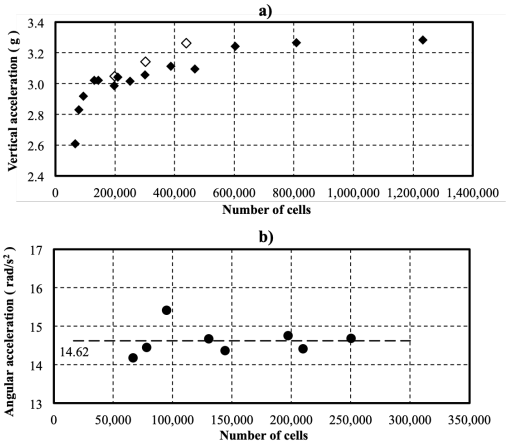

Fig 8 Mesh refinement with vertical acceleration peaks (a): not filled diamonds for custom volumetric control, and solid diamonds for base size; mesh refinement with roll angular acceleration peaks (b).

Reproducing roll motion on the boat during an impact has been one of the main objectives of the study. So peak roll angular acceleration was used to validate the meshing refinement process in a similar manner as the peak vertical acceleration. Fig 8b shows that the peak angular acceleration converges to about 14.62 rad/s^2 as the mesh becomes finer and the number of cells grows. It can be appreciated that even for a relatively course mesh of 200 thousand cells, the deviation is not far from the convergence. Therefore, it is decided to

incorporate the refinement for a roll validation within the general vertical refinement procedure. After the refinement stage, the mesh can be displayed as following Fig 7b. Fig 7b illustrates the mesh arrangement around the boat hull, according to the mesh refinement volumes. The mesh shown in Fig 7c above simulates the drop very well.

6) Time step

The peak acceleration that occurs at a very short period strongly depends on the solver time step size, which in turn affects the number of iterations required per second. The simulation accuracy increases with decreasing time steps.

$$\text{Number of iteration per second} = 1 / \text{time step} \quad (23)$$

To determine a suitable time step, the simulation is tried using a flat entry angle and a drop height of 1 metre with mesh size of 440k cells. Figure 9a shows the effect of the time step on impact acceleration.

The peak acceleration increases with smaller time steps. The bigger the time steps are the earlier the peak would occur. The impact peak for a 1-metre drop takes place around 0.45s after the release according to theoretical calculation. Fig 9b shows the trend of the peak acceleration with varying time steps with the shortest time step of 0.0005 s in addition to the first four steps presented in Fig 9a.

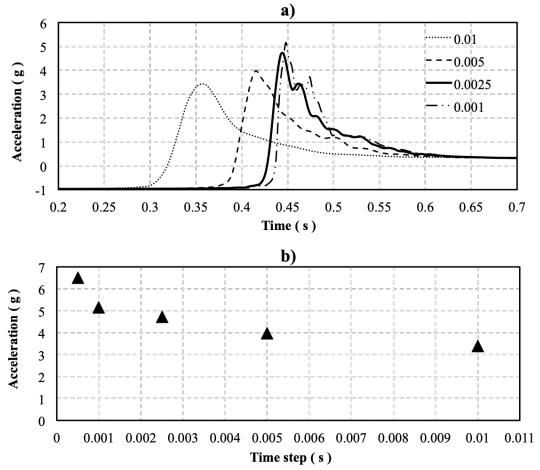

Fig 9 Vertical z-axis acceleration time histories at the centre of mass (CoM) with a 1-m drop height with four time steps in seconds is presented in (a); peak vertical accelerations are plotted against the four time steps (a) and an additional step of 0.0005 s in (b).

Smaller time steps lead to higher peak accelerations. The smallest time step investigated of 0.0005 s results in a vertical acceleration of 6.5g. However, the computational time for this simulation is around 15 hours. As a computational compromise, the time step is set to 0.0025 s with the fixed mesh size, giving rise to a computational time of around 6-8 hours with about 400 iterations per simulated second resulting in a smaller peak acceleration of 4.5g. We note that using this resolution will result in a reduced peak acceleration, but it saves significant computational effort over the many simulations in the work reported later.

III. Results

The boat drop simulation requires setups of the inertial property for the DBFI computation, the initial flat entry, and the initial roll angle entry. This section starts to introduce these configurations first, and then the sub-sections present the results for flat entry and roll entry simulations.

Inertial properties of the boat: mass, centre of mass, mass moments and products of inertia are needed to derive dynamic loads on the rigid boat. These depend on how the boat is loaded by the crew, passengers, and equipment. The present study assumes that three crew members are seated on the three seats illustrated in Fig 1 with 1825 kg as the total mass of the lifeboat. The position of the centre of mass (CoM) is estimated from [12]: x position = 2.523 m (from the stern), y position = 0 m, and z position = 0.168 m (from the lowest keel) using the coordinates in Fig 3 and 4. As the mass distribution of the boat is symmetric about the three orthogonal axes and the primary interest of investigation is translational vertical (z), rotational roll (φ), and translational lateral (y) motion, only mass moments of inertia are required to derive the deck motion treating the entire boat-crew system as a rigid body [12]: I_{xx} = 300 kg m^2, I_{yy} = 2500 kg m^2, and I_{zz} = 2600 kg m^2. The products of inertia are not required.

The flat entry simulations are designed to examine vertical acceleration during different drop heights. The DFBI model is limited to move only in the global vertical Z-axis to investigate the declaration during the entry phase. It is expected that the vertical acceleration at the CoM increases with increasing drop height (Table III). s

TABLE III. Flat entry drop heights

Drop height (m)	Impact velocity (m/s)
0.5	3.132
1.0	4.429
1.5	5.425
2.0	6.264
2.5	7.004

The roll entry simulations analyse the influence of the initial roll entry angle at impact. The DFBI model can translate in the global Z- and Y-axes and rotate about the X-axis. The transferrable reference frame can be used to derive translational motion and loading on occupants at various seating position on the deck. The selected entry roll angles are combined with shorter list of drop heights (Table IV). Due to the larger impact area and therefore greater flow resistance the vertical acceleration is expected to be higher with a larger roll entry angle φ. The boat also experiences considerable angular acceleration about the CoM in the longitudinal x-axis (Fig 4).

TABLE IV. Roll entry angles and drop heights

Drop height (m)	Roll entry angle (degrees)
0.5	5, 10, 15, 20, 25
1.0	5, 10, 15, 20, 25
2.0	5, 10, 15, 20, 25

The kinematics of primary interest derived in the local (boat) body coordinate system (Fig 3 and 4, Table I) are the vertical translation (z), lateral translation (y) and roll (φ). The results are presented firstly with flat entry and then with roll entry angle with more focus on the latter.

A. Flat entry

During flat entries, the time gaps between the peak acceleration, velocity and displacement time histories at the CoM of the boat with varying drop heights H conform to a quadratic relationship (Fig 10). The velocity peaks after the freefall phase during the impact phase the displacement peaks during the inertial phase (Fig 2). By extracting the peak accelerations and peak displacements from Fig 10, Fig 11 illustrates their trends with respect to the drop height. The peak acceleration seems to match a linear trend line (Fig 11a), while the peak displacement exhibits a more logarithmic trend (Fig 11b). A drop height of 0.5 m results in a hull dive around 0.62 m beneath free water surface, a drop height of 2.5 gives a dive of about 0.77 m. The static draft of the boat settles at around 0.37 m below water. The peak acceleration reaches 1.98, 4.30, 6.36, 8.35 and 10.38 g for the five drop heights respectively.

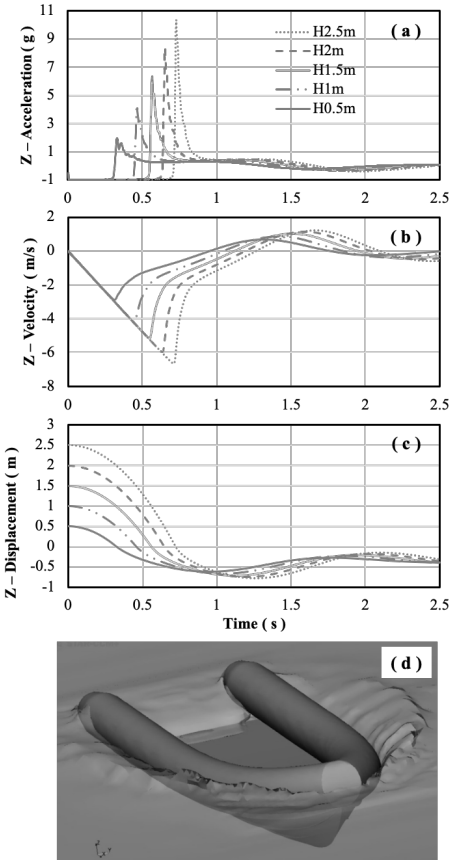

Fig 10 Time histories of vertical z-axis acceleration (a), velocity (b), displacement (c) at the CoM of the boat with the five drop heights H, and a frame of a 2.5m drop (d).

B. Roll angle entry

The vertical (z) and lateral (y) translational accelerations are governed by the angular roll acceleration (φ) about the x-axis at the CoM of the boat defined by Eq (15), (16) in Fig 4.

1) Angular acceleration

The effects of three drop heights (0.5, 1.0 and 2.0 m) and five initial roll entry angles (5, 10, 15, 20 and 25 degrees) on the angular acceleration time history is presented in Fig 12. The three main inverted peaks indicate the three drop heights. In each of the three groups, the angular acceleration tends to increase polynomially with increasing initial roll angle.

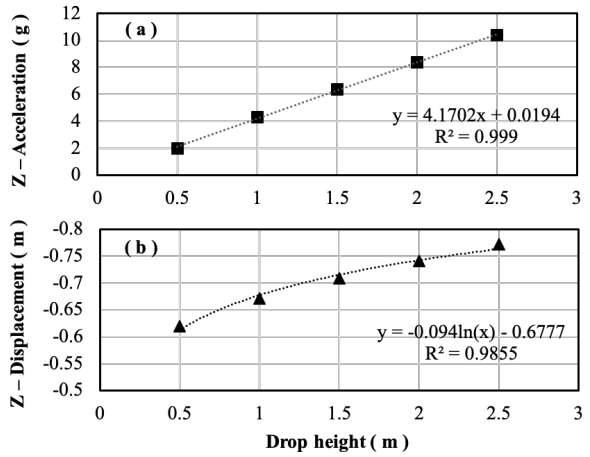

Fig 11 Vertical z-axis peak acceleration (a) and peak displacement (b) at the CoM of the boat with the five drop heights with trend lines and a measure of regression.

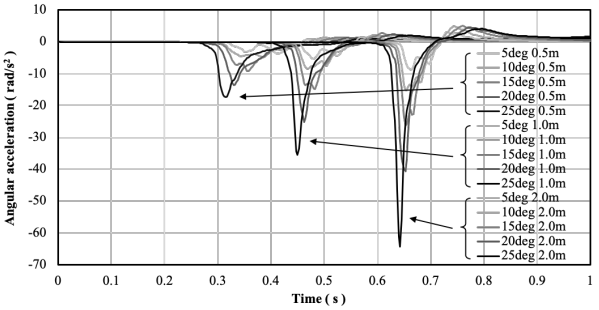

Fig 12 Roll angular acceleration time histories of the boat for the three drop heights and five roll entry angles.

The drop heights at varying roll entry angle seem to be linearly correlated to the peak angular roll acceleration (Fig 13a). At each given drop height, increasing initial roll angle results in an increase in peak roll angular acceleration following a 3rd order polynomial trend (Fig 13b). This contrast highlights the importance of entry roll angle in assessing the resultant shock motion on the boat.

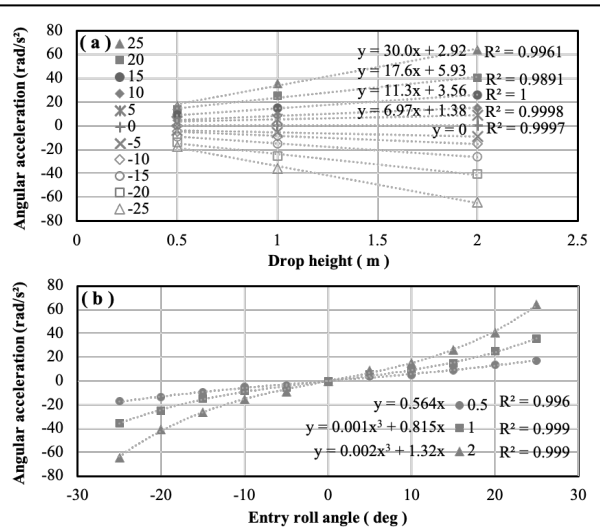

Fig 13 Peak roll angular acceleration of the boat for the three drop heights and five (eleven if taken symmetrically) initial roll entry angles [-25, 25] deg.

2) Vertical acceleration

The peak vertical acceleration $\ddot{z}(t)$ in Eq (15) at the CoM with varying entry roll angles and drop heights can be approximated by a group of 4th order polynomial lines (Fig 14a). With a drop height over 1 m, the peak acceleration increases with increasing entry roll angle.

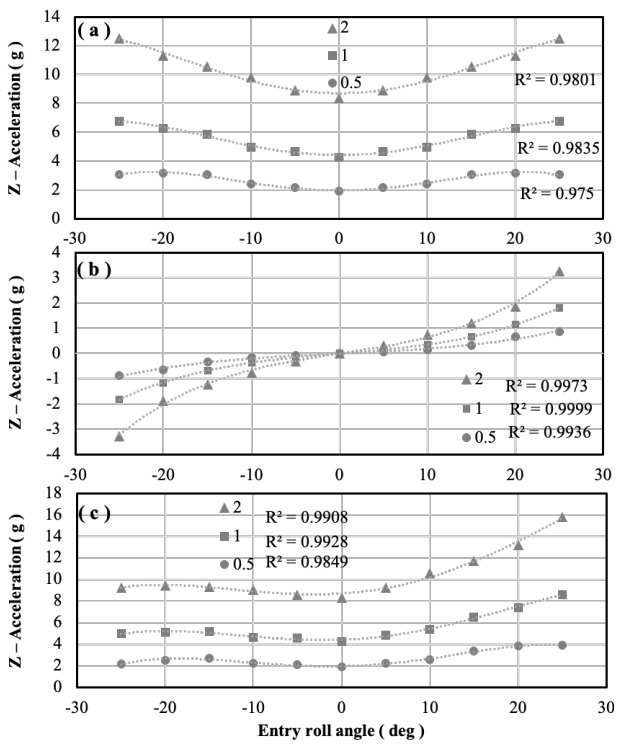

Fig 14 Peak linear vertical component (a), peak angular component (b) and total peak vertical accelerations (c) at the right crew seat position with reference to Fig 4a.

The peak vertical acceleration component caused by angular acceleration $\ddot{\varphi}(t) \cdot d_y$ in Eq (15) with $d_y = \pm 0.5$ m from the CoM representing the right crew seat position (Fig 1) at varying entry roll angles and drop heights can be approximated by a group of 3rd order polynomial lines (Fig 14b). The vertical acceleration component varies in the negative and positive region following the free-body diagram in Fig 4a.

Summing the linear $(\ddot{z}(t))$ and the angular $(\ddot{\varphi}(t) \cdot d_y)$ components of the vertical acceleration, Fig 14c shows the total peak vertical acceleration at the right crew seat position (Fig 1) for the range of entry roll angles and drop heights using a series of 4th order polynomial lines. For a positive entry roll angle, the peak acceleration of the right crew seat position increases with increasing entry angle.

The percentage change of the total peak acceleration for different entry roll angles show an increase of up to 28% between a 0 deg and 25 deg entry angle (Fig 15). The percentage change seems to be independent of drop height and follows a cubic trend line.

3) Lateral acceleration

Similar to the vertical acceleration analysis, the results are given for the CoM lateral acceleration, the lateral acceleration caused by angular acceleration and the combined total lateral acceleration. The peak lateral acceleration $\ddot{y}(t)$ in Eq (16) at the CoM with varying entry roll angles and drop heights can be approximated by a group of linear fit lines (Fig 16a). As the absolute entry roll angle increases, the absolute lateral acceleration at CoM also increases.

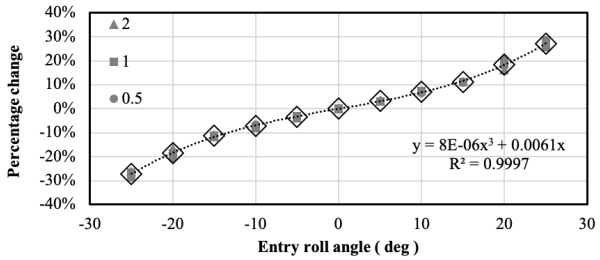

Fig 15 Percentage change in total vertical acceleration for the three drop heights and five initial roll entry angles (eleven if taken symmetrically) with hollow diamonds showing the average of all three drop heights.

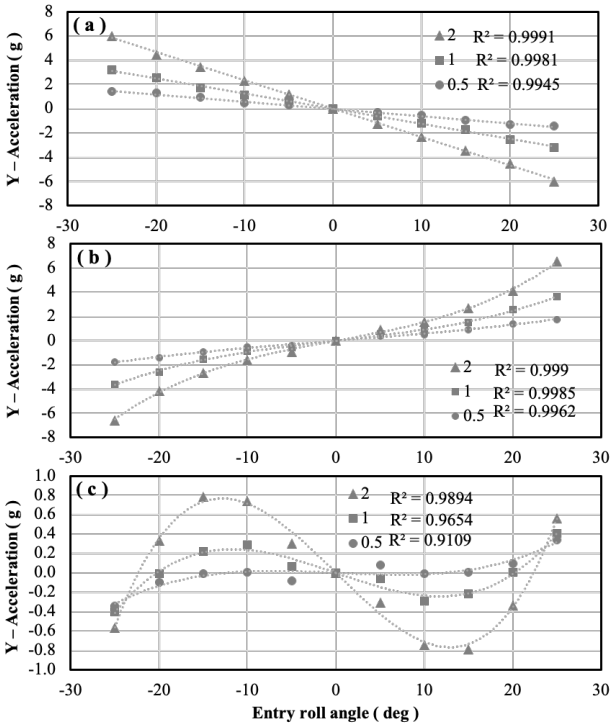

Fig 16 Peak linear lateral component (a), peak angular component (b) and total peak lateral accelerations (c) at a crew seating height of 1 m above boat CoM (Fig 4a).

The peak lateral acceleration component caused by angular acceleration $\ddot{\varphi}(t) \cdot d_z$ in Eq (16) with d_z = 1 m above the boat CoM representing the crew CoM in a right seating position (Fig 1) at varying entry roll angles and drop heights can be approximated by a group of 3rd order polynomial lines (Fig 16b). The lateral acceleration component varies in the negative and positive region according to the free-body diagram in Fig 4b. Notably, the angular acceleration caused lateral component increases with increasing roll entry angle from -25 to 25 deg, while the translational lateral acceleration at CoM decreases.

Summing the linear $(\ddot{y}(t))$ and the angular $(\ddot{\varphi}(t) \cdot d_z)$ components of the lateral acceleration, Fig 16c shows the total peak lateral acceleration at the height of the crew seat position (d_z = 1 m, Fig 1) for the range of entry roll angles and drop

heights using a series of 3rd order polynomial lines. It is clear that the dominant translational lateral component is cancelled largely by the angular acceleration caused lateral component, giving rise to the maximum total lateral acceleration of 0.8 g at an entry roll angle between 10 and 15 deg. Around this entry angle, drop height or impact velocity has the dominant effect on the total lateral acceleration experienced by the crew. The lateral acceleration is zero at 10 deg for 0.5m drop height, 20 deg for 1m drop height and around 22 deg for 2m drop height.

IV. Discussions

In most cases the dominant influence on vertical acceleration has been the vertical drop height, which shows a linear behaviour in terms of peak acceleration. The roll angular acceleration is affected by both drop height and entry roll angle. Lateral acceleration has been moderate, with a peak magnitude of less than g, mainly due to the "cancelling effect" between the translational inertial component and the angular centrifugal component. This section will discuss the main limitations of the study and then move on to examine the resultant accelerations in the flat entry and roll angle entry scenarios.

A. Limitations

In reality, be it a transit or a controlled drop, it is difficult to reproduce the multi-axial motion during the flat entry and roll angle entry cases. Environmental factors such as the wind and waves, boat performance and measurement instruments can all affect the motion acquired for validation [2, 6]. The obtained simulation results can only be used as a reference to the nominal conditions. It is important to recognise that asymmetry from the boat mechanical system, and the environment during the impact can all affect the translational and rotational motions in the frontal plane. The simulations are designed to estimate the range of the multi-axial motions using two independent variables: the drop height and the entry roll angle. The roll, vertical and lateral motions are assumed to be the dominant kinematic output in the frontal plane derived from the fluid-structure interaction model. Pitch, yaw and fore-and-aft motions are likely to increase dramatically if there is any asymmetric characteristics on the boat and the wave right from the beginning of the impact. Motion measured during drop test and sea trial can be used to validate the simulation.

In the present study, the boat just drops into the water without any initial motion in the longitudinal direction relative to the flow surface. The STAR-CCM® has facility to model fifth order waves that can be part of the longitudinal motion of the boat. This could be used to represent a suitable forward planing velocity of the lifeboat in addition to the fall.

Simulation parameters such as the mesh size and the time step size need to be determined by trialling and comparing the peak acceleration for a flat entry drop. With a fixed small time step, the refinement should see the peak magnitude to converge. For computational efficiency reasons, the time step was chosen to be 0.0025 s, which resulted in a computational time of approximately 6 hours for each simulation. With increased computational resources, the accuracy can be improved using smaller time steps of 0.0001 s and lower. Such values will capture the peaks to a higher degree of accuracy. In addition finer resolution in the meshes will improve accuracy, but at an additional computational cost.

The physical models employed by this project were developed considering free falling bodies entering water [3, 7]. The κ-ε-Turbulence has been used for this application, but the use of other turbulence models warrants further consideration.

B. Flat entry

With an increasing drop height and an ensuing rising initial impact velocity, the peak vertical acceleration of the lifeboat increases steadily. It is difficult to make comparisons between a symmetrical and asymmetrical wedge as the Atlantic 21 hull has a flat section in the frontal plane at the bottom (Fig 3). This influences the impact behaviour and cannot be determined by an analytical model. So the analytical solution of the pressure distribution around the hull using [3] does not apply as the pressure variation introduced by the flat bottom was not taken into account. The peak acceleration magnitudes generated from the present numeric simulation seem to be comparable to those measured during the sea trials using a different boat [13]. A similar free-fall drop test at drop heights of 0.5 and 1 m conducted in real-life with the smaller RNLI D-class lifeboat showed doubled peak acceleration values in the vertical direction at the location with a deadrise angle of 15 deg [2]. As this measurement location is close to the boat CoM, it is plausible that the hull form, i.e. the D and A21, dramatically affect the peak vertical acceleration. With no experimental result of the same boat to validate at least one simulation solution, it is difficult to evaluate the absolute motion. However, the effects of varying drop height seems to match those measured in controlled tests [2] and sea trials [13].

C. Roll angle entry

The angular acceleration caused by the initial entry roll angle greatly influences the peak translational accelerations in both lateral y- and vertical z-axes of the boat but in different ways.

With an entry roll angle, the overall lateral acceleration is comprised of the lateral acceleration at the boat CoM and the lateral component caused by the angular acceleration of the boat. Separately, the lateral acceleration at the CoM can reach up to 6g. However, the sitting position offset in the lateral y-axis gives rise to an angular acceleration and an ensuing lateral acceleration component counteracting the lateral acceleration at the boat CoM. As a result, the CoM lateral component is almost cancelled by the angular acceleration induced lateral component. The maximum value found is around 0.8 g with a drop height of 2 m under an entry roll angle of 10 to 15 deg.

A crew member sitting out of line of the central line of the boat will experience the same magnitude of y-axis lateral acceleration no matter if they are at the left or right of the central line (Fig 16c); a right side sitting position (see Fig 1b) will result in a considerably larger z-axis vertical acceleration comparing to a left sitting position if an initial entry roll angle is positive about the x-axis of the boat (Fig 14c). By considering a crew member to the right of the boat central line (Fig 1b), it is necessary to include the vertical acceleration caused by the angular acceleration. Combining the vertical acceleration with an offset of +0.5 m in the lateral y-axis results in an increase in acceleration of up to 28% compared to that at the boat CoM. On the contrary, combining the vertical acceleration with an offset of -0.5 m in the lateral y-axis decreases the overall vertical acceleration proportionally. This percentage change is found to be almost independent of

drop height (Fig 15). At a fixed entry roll angle, both lateral and vertical accelerations increase with increasing drop height almost linearly.

The z-axis vertical acceleration at the boat CoM is the most dominant value to describe the behaviour of the mechanical shock during a drop slam. The entry roll angle increases the vertical acceleration dramatically. With zero roll angle, the hull wedge can expel fluid equally form both sides in the frontal plane; however, if a roll angle is introduced, the pressure field is asymmetric and higher on the tilted hull forming a horizontally flatter surface giving rise to higher drag coefficient – compare Fig 3 a and b. The drag coefficient is expected to be much higher for an asymmetric roll entry. To work with estimated measurements of the boat hull geometry, it is often useful to approximate those values with a trend line. This works well within the considered entry roll angle range as the hull shape is an almost regular triangle. However, in reality the inflated tube as part of the hull structure can influence the solution. The maximum vertical acceleration is expected when the impact angle is equal to the deadrise angle – a flat plate entry.

V. Conclusions

The present study demonstrates how to utilise the dynamic fluid body interaction facility in an off-the-shelf CFD package to simulate wave slam induced mechanical shocks on a RIB planing lifeboat. A typical combination of drop heights and a range of initial entry roll angles leading up to the deadrise angle are investigated. The mesh size and integration time step size are found to affect the numeric simulation solution where a compromise between total simulation time (along with computational power) and accuracy has to be determined. The multibody motion derived at various locations on the boat allows evaluation of any human factors design intervention for shock mitigation on fast craft without the time and logistic cost for field trials.

The vertical acceleration calculated at an offset crew seat is considerably higher than that at the boat CoM in the frontal plane. The percentage increase from the offset position relative to the CoM is primarily governed by the entry roll angle with little influence from the drop height. This is a wakening message to craft designers, human factors specialist and seating manufacturers that conventional testing regimes of uniform vertical drop tests may not be adequate enough to take into account the high acceleration events caused by asymmetric entry angles, be it roll, pitch or yaw. Hence, any claimed protective equipment for mechanical shocks on planing craft needs to consider non-uniform entry situations.

The simulation reveals that the lateral acceleration is less critical when assessing mechanical shocks in the frontal plane of the lifeboat. The lateral component at CoM is largely cancelled by the lateral component due to the offset and the angular acceleration, producing a magnitude less than 1g for all entry angles with drop heights of 2m or less.

At any fixed entry roll angle, increasing drop height tends to increase linearly the translational lateral and vertical accelerations at the boat CoM, and the angular acceleration due to the initial entry roll angle. This allows one to derive motions anywhere on the boat, assuming that the boat retains its rigid body inertial and geometric properties. Such assumption may not be true if the inflatable tubes of the lifeboat becomes noticeably deformable due to extremely high magnitudes of pressures during large shocks. However, the effect is expected to be reduced due to the 'cushioning effect'.

The study can be extended to apply more realistic sea conditions including a propagating wave and a 6-DoF simulation with different entry pitch and yaw angles of the boat. This can further confirm the speculation whether and how any initial entry boat angle can dramatically increase the vertical boat acceleration.

References

[1] Y Huang (2018). Preliminary laboratory study of dynamic sitting and mechanical shock on high-speed planning boat coxswain. 53rd UK Conference of Human Responses to Vibration, Ascot.

[2] PK Halswell, PA Wilson, DJ Taunton, S Austen (2016). An experimental investigation into whole body vibration generated during the hydroelastic slamming of a high speed craft. Ocean Engineering 126, 115-128.

[3] R Zhao, O Faltinsen (1993). Water entry of two-dimensional bodies. Journal of Fluid Mechanics 246, 593–612.

[4] E-M Yettou, A Desrochers, Y Champoux (2005). Experiments on the water entry of asymmetric wedges using particle image velocimetry. Fluid Dynamics Research 38, 47-66.

[5] MR Riley, T Coats, K Haupt, D Jacobsen, (2010). The Characterization of Individual Wave Slam Acceleration Responses for High Speed Crafts. The 29th American Towing Tank Conferece. Norfolk: The Comlumbia Group.

[6] NC Townsend, PA Wilson, S Austen (2008). What influences the motions of rigid inflatable crafts. Southampton: Proffesional Engineering Publishing.

[7] SR Johannessen (2012). Use of CFD to Study Hydrodynamic Loads on Free-Fall Lifeboats in the Impact Phase. Trondheim: NTNU-Trondheim.

[8] JN Newman (1977). *Marine Hydrodynamics.* Cambridge, USA: MIT Press.

[9] C Fletcher (1998). Computational Techniques For Fluid Dynamics 1: Fundamental & General Techniques, Springer-Verlag, Berlin.

[10] WJ Rider, DB Kothe (1998). Reconstructing Volume Tracking. Journal of Computational Physics, 112-152.

[11] CD-Adapco (2016). STAR-CCM User Guide. Melville: Siemens.

[12] SG Lewis, DA Hudson, SR Turnock, JIR Blake & RA Shenoi (2007). A comparison of experimental measurements of high-speed RIB motions with non-linear strip theory, Australian Journal of Mechanical Engineering, 4:2, 165-182.

[13] Kearns, SD (2001). Analysis and Mitigation of Mechanical Shock Effects on High Speed Planing Boats. Cambridge, USA.